Desalination and Water Treatment
www.deswater.com

doi: 10.1080/19443994.2013.831793

52 (2014) 7531–7542
December

Taylor & Francis
Taylor & Francis Group

Synthesis, structural characterization, electrochemical, and electrical study of polystyrene-based manganous tungstate composite cation exchange membrane

Mohd Arsalan, Rafiuddin*

Membrane Research Laboratory, Department of Chemistry, Aligarh Muslim University, Aligarh 202002, India
Tel./Fax: +91 571 2703; email: rafi_amu@rediffmail.com

Received 27 April 2013; Accepted 19 July 2013

ABSTRACT

The polystyrene-based manganous tungstate composite membrane was prepared by applying sol–gel method. The membrane was characterized by Fourier transform infrared spectroscopy, X-ray diffraction, thermogravimetric analysis, differential thermal analysis, scanning electron microscopy, and (LCR) study. Membrane was found to be crystalline, the arrangement of particle was uniform, and there were no sign of visible breakage or cracks. The theoretical value of potential was determined by Teorell–Meyer–Sievers, method and the electrochemical property was measured by a potentiometer. From observation, it is clear that the membrane potential increases with decreasing the concentration of electrolytes and the charge density follows the reverse order of potentials. By observing transport number the mobility ratio, distribution coefficient, and charge effectiveness can be calculated very easily.

Keywords: Inorganic compounds; Polymer; Sol–gel chemistry; X-ray diffraction; Mechanical and electrical properties

1. Introduction

A great number of ion-exchange membranes have been widely studied due to their versatile applications in chemical industries, food, drugs, wastewater treatment, and in many separation processes [1]. Furthermore, the ion-exchange composite membranes find applications in various processes such as electro-dialysis, desalination, diffusion, electro-deionization, membrane electrolysis, electrochemical synthesis, fuel cells, and storage batteries also. Therefore, they are useful in pollution control, energy saving, power generation, resource recovery, etc [2].

Such composite membranes have also been used in electro-dialysis for briny water desalination. To do that, ion-exchange membranes should possess high selectivity and conductivity. Separation of solutes by a neutral membrane takes place due to the differences in solute sizes and their interactions with the membrane. But charged membrane can separate the solutes or ions according to their nature. Nowadays it is very necessary to investigate the ions transportation specifically in aqueous, organic, and electrolyte solutions system across a charged membrane from the perspective of medical and industrial applications [3].

Recently the electro-dialysis is one of the very important applications of ion-exchange membrane processes which suggested the technique to remove

*Corresponding author.

heavy metals and other inorganic toxic substances which were generated by the electroplating processes. From the industrial application point of view, the electro-dialysis process is useful to know the electrochemical performance of the ion-exchange composite membranes, their conductivity, selectivity, stability, and ion transport number [4–7]. The inorganic–organic composite membranes are developed by mixing organic polymers and inorganic particles together in a specific ratio. Therefore, these membranes exhibit the ideal properties of both the constituents [8].

From the study, it is clear that polystyrene is a good binder to make a compact and rigid framework. Therefore, in this study we have used the above organic polymer with the inorganic tungstate to give a stable membrane from the economical and industrial point of view [9–14]. The measurement of membrane potential is an important phenomenon to characterize the transport property across a charged membrane [15]. Theoretically, the membrane potential of a charged membrane in aqueous electrolyte solution system developed by Teorell–Meyer–Sievers (TMS) method can be treated by Donnan equilibrium theory and the Nernst–Planck equation. So, it is assumed that the fixed-charge groups are homogeneously distributed in the membrane [16]. The value of mean activity coefficient of the electrolytes in the external solution is negligible. Henderson solved the Nernst–Planck equation at the constant ion concentration gradient.

In this study, the membrane potentials of different aqueous electrolyte systems are measured and applied to the theoretical equation, which is based on the Donnan equilibrium and the Nernst–Planck equation and it is considered that the effect of electrolytes in the external solution is due to the mean activity coefficient and it is the same in the membrane as well as solution phase at each interface must also be made [17]. The diffusion potential depends on the mobility of ions in the membrane, and it affects the transport property of ions. The Donnan potential of the membrane depends on the charge density, which plays a significant role in the selectivity of the ions with respect to their ionic nature.The measurement of the diffusion potential and Donnan potentials will give the important parameters that are the ionic mobility, effective charge density, etc [18,19].

The surface charge density D^- is the fundamental parameter which controls the membrane phenomenon and it was calculated by observed and theoretical membrane potential values of different electrolytes by TMS method. Some other parameters including distribution coefficient, transport numbers, mobility ratio, charge effectiveness etc. were also calculated by the above-used method [20].

2. Materials and methods

2.1. Chemicals used

Pure crystalline polystyrene (Otto Kemi, India, AR) ground and sieved through 200 meshes was used as a binder, 0.2 M sodium tungstate solution (E. Merck India with a purity of 99.90%), 0.2 M manganous chloride ($MnCl_2$) solution (Otto Kemi, India), and various electrolytes solutions (KCl, NaCl, and LiCl) of different concentrations were also arranged.

2.2. Instruments

Scanning electron microscopy (SEM) images were taken by scanning microscope Leo 4,352 at an accelerating voltage of 20 kV. The phase transformation analysis of the sample was conducted by XRD-Miniflex-II X-ray diffractometer "Rigaku Corporation" with Cu Kα radiation. Infrared spectrum was recorded by using an "Interspec-2020 Fourier transform infrared spectroscopy (FTIR) spectrometer" spectrolab UK. Thermogravimetric analysis (TGA) and differential thermal analysis (DTA) analysis of the sample was carried out by "Shimdzu DTG-60H", whereas, the dielectric property of the sample was determined with "Agilent-Model 4284A" precision LCR meter.

3. Experimental

3.1. Preparation of manganous tungstate material

Manganous tungstate was prepared by sol–gel [21] or co-precipitation process by mixing the 0.2 M aqueous solution of sodium tungstate with 0.2 M manganous chloride solution by a constant stirring of 1–2 h and after the stirring process pH of the precipitated solution must be maintained. The resulting precipitate was well washed almost 4–5 times by double-distilled water to remove free electrolytes and dried the material till the 3–5 h at 100˚C. After that, it will be powdered with the help of pestle and mortar, until the size should be less than 200 meshes. Pure crystalline polystyrene was also ground and sieved through 200 meshes.

3.2. Preparation of polystyrene-based manganous tungstate composite membrane

The precipitate was mixed with polystyrene granules by pestle and mortar and then, the mixture was kept into a cast die having a diameter of 2.45 cm and placed in a digital furnace by maintaining a temperature of 200˚C till 1–2 h to equilibrate the reaction mixture. After that, the material will be transferred to a pressure device "SL-89, UK" to apply pressure of

100 MPa for the fabrication of the membrane. By embedding 25% polystyrene, the prepared membrane was found to be more mechanically stable, and gave reproducible results. If the amount of polystyrene is greater or lesser than the 25%, it cannot make the appropriate stability for membrane. So the total amount of the mixture utilized for the preparation of the membrane contained 0.125 g of polystyrene and 0.375 g of manganous tungstate material. After that, the prepared membrane was subjected to microscopic and electrochemical examination to check for cracks and homogeneity of the membrane surface. After all the composite membrane should be placed for potential observation by carefully controlling the condition of fabrication [22].

3.3. Physico-chemical characterization of composite membrane

3.3.1. Measurement of thickness and swelling

The thickness measurement of membrane is obtained by the average thickness of 4–5 replicates by using screw gauze apparatus and swelling is measured as the difference between the average thickness of the membrane equilibrated with 1 M NaCl for 24 h and the dry membrane.

3.3.2. Measurement of water absorption and water flux

The water absorption in the membrane was calculated by the following equation:

$$\%\ \text{Total}\ (\text{weight}_{\text{wet}}) = \frac{W_{\text{w}} - W_{\text{d}}}{W_{\text{w}}} \times 100 \quad (1)$$

where W_{w} is the equilibrium weight of the swollen membrane, which is obtained by soaking in water for 5 h, and W_{d} is the weight of the dry membrane. The pure water flux can be measured under a pressure difference of 0.2 MPa at an ambient temperature, and it can be calculated by the following equation [23].

$$F = V/At \quad (2)$$

where V is the total volume of the water permeated during the experiment, t is the operation time, and A is the membrane area.

3.3.3. Water content (% total wet weight)

The membrane was first kept in water for soaking, for the water to diffuse the salt, and after that it was blotted quickly with Whatman filter paper to remove the moisture from the surface, and then immediately weighted. These membranes were further dried to attain a constant weight in vacuum, over P_2O_5 for 24 h. The water content (total wet weight) of the membrane was calculated as:

$$\%\ \text{Total}\ (\text{weight}_{\text{wet}}) = \frac{W_{\text{w}} - W_{\text{d}}}{W_{\text{w}}} \times 100 \quad (3)$$

W_{w} = weight of the soaked membrane and W_{d} = weight of the dry membrane.

3.3.4. Porosity

Porosity is the volume of incorporated water in the cavities of the membrane per unit volume from the water content data:

$$\text{Porosity} = \frac{W_{\text{w}} - W_{\text{d}}}{AL\rho_{\text{w}}} \quad (4)$$

W_{d} = weight of dry membrane, A = area of membrane, L = thickness the membrane, ρ_w = density of water.

3.3.5. Chemical stability

Chemical stability was determined by ASTM D543-95 procedure. It will analyze the morphological changes that include alteration in color, texture, brightness, decomposition, and splits through which the membrane was exposed to different acidic and basic media and evaluated after 24, 36, and 48 h.

3.3.6. SEM investigation

By SEM analysis, the morphology of the membrane was investigated through Leo 4352 at an accelerating voltage of 20 kV. The sample was mounted on a copper stub and sputter coated with gold to minimize the charging, and was used to verify the microstructure of fabricated porous membrane.

3.3.7. XRD analysis

XRD pattern of the polystyrene-based MT composite membrane was recorded by Miniflex-II X-ray diffractometer "Rigaku Corporation" with Cu Kα radiation.

3.3.8. FTIR spectra of composite membrane

The FTIR spectrum of pure polystyrene and polystyrene-based MT composite membrane was done by

"Interspec 2020 FTIR spectrometer" spectrolab UK. The sample compartment was 200 mm wide, 290 mm deep, and 255 mm high. The entrance and exit beam of sample chamber was sealed with a coated KBr window, and there was a hinged cover to seal it from the environment.

3.3.9. The thermal stability of the membrane

The degradation process and thermal stability of polystyrene-based MT composite membrane was investigated by TGA "Shimadzu DTG-60H" under nitrogen atmosphere by using a heating rate of 20 °C min^{-1} from 25 to 800 °C.

3.4. Observation of membrane potential

With the help of digital potentiometer "Electronics India 118", the potential of membrane can be obtained through which the membrane was placed in the centre of the measuring cell which is having two compartments of definite size [8,24]. Mainly KCl, NaCl, and LiCl electrolyte solutions were used and it was prepared by deionized water. The collar-shaped measuring cell was used for injecting the electrolyte solutions, and it was stirred by a magnetic stirrer. The membrane potential was determined with the help of potentiometer of reference electrodes (SCE), which was kept dipped into the both chamber of different concentrated solutions. All the observation of ionic potential was made at room temperature. The electrochemical setup which was used for membrane potential measurements may be depicted as follows and presented as in Fig. 1.

3.5. Dielectric properties of the composite membrane

The dielectric and impedance measurements were made from 75 to 5 MHz using Agilent "Model-4284A" precision LCR meter.

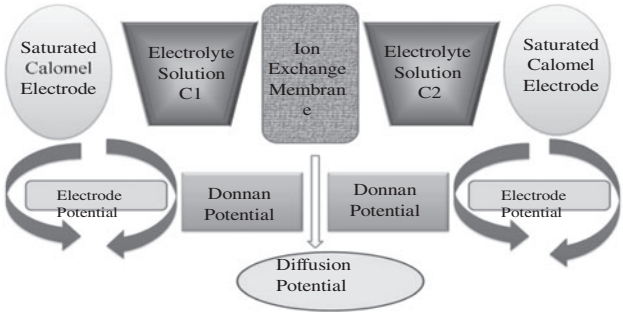

Fig. 1. Electrochemical setup of potential determination.

4. Result and discussion

The surface of the membrane was investigated by SEM characterization which is shown in Fig. 2 and was prepared at 100 MPa [25,26]. The distribution of materials that is polystyrene and MP was uniformly mixed in the medium, and therefore, it is clear that the prepared membrane has homogeneous nature to show good result and it is applicable for further observation.

For the XRD analysis, the sample should be in powdered form and was mounted on the sample holder with the help of a glass slide. The pattern was recorded by using the Cu Kα radiation ($\lambda = 1.54060$ A°) in 2θ ranging from 20° to 80° to show the structure and lattice parameters of the sample. The XRD spectrum of polystyrene-based MT is depicted in Fig. 3, which tells the lattice constants of the sample was found to be as (a) 5.758 A° and (c) 9.443 A°. The pattern of particles showed two most intense peak at $2\theta = 28.30°$and 51.50° which corresponds to (211) plane of polystyrene-based MT material. [27]. The crystallite size of the sample was found to be ~26.8 nm calculated from the most intense peak, and these peaks in the spectra show that the particles were present in the crystalline form.

FTIR spectrum was used to analyze the structural properties and the bonds of the sample. Fig. 4 shows the FTIR spectrum of pure polystyrene and polystyrene-based MT composite membrane. The spectrum shows two strong IR absorption bands at ~676.23 and 814.30 cm^{-1} due to the H–O–H bending of the H_2O molecules or the polystyrene compound. The fundamental frequency at ~504.51–546.23 cm^{-1} arises due to hindered rotations of the hydroxyl ions or the tungstate group of the material. The band shown at 3,404 cm^{-1} is due to the water molecule which comes from the atmospheric moisture or by the KBr pallets used during the recording of FTIR spectrum.

The TGA and DTA curves of membranes are shown in Fig. 5. As can be observed from the TGA curves of the polystyrene-based MT membrane that there was a 2.27 mg (33.076%) weight loss that took place at the ~600 °C temperature. However, most of the composite membrane did not have any weight loss. By taking the reference of TGA it is clear that the polystyrene-based MT membrane had a high hydrophilicity nature and could absorb moisture from the surrounding air.

Fig. 6(a) shows the complex impedance plot of sample. Generally, the grains are effective in high frequency region, while the grain boundaries are effective in low frequency region. Thus, the circular arc appearing in the high frequency region

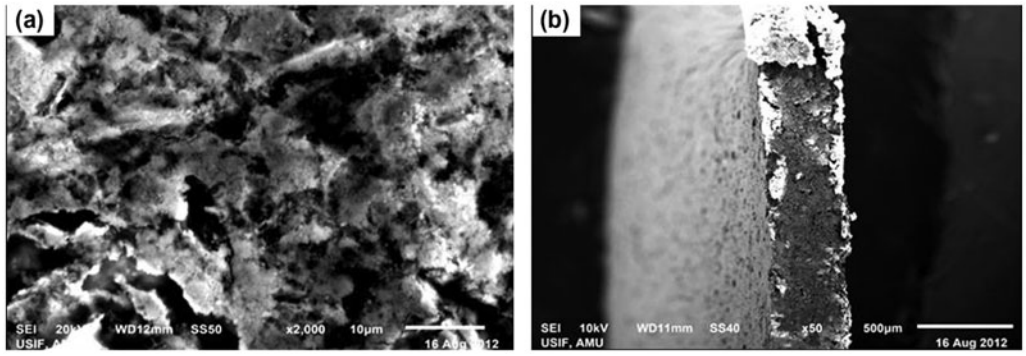

Fig. 2. SEM images of polystyrene based MT composite membrane. (a) Surface image. (b) Cross-sectional view.

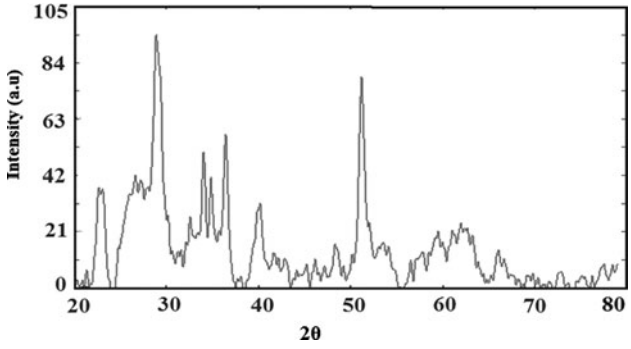

Fig. 3. XRD spectra of the polystyrene based MT composite membrane.

corresponds to grain contribution, while the low frequency region corresponds to grain boundary contribution. It is evident from the plot itself that the figure shows single circular arc behaviour, which suggests the predominance of grain boundary resistance over the grain resistances in this sample. Due to this fact, the single circular arc is being observed in Cole–Cole plots. Moreover, it can be seen from above graph.

Fig. 6(b) shows the variation in dielectric loss factor with frequency at room temperature. It is observed that tan δ decreases with the increase in frequency for the characterized sample, which may be due to the space charge polarization. It is considered to be caused by domain wall resonance. At higher frequencies, the losses are found to be low since domain wall motion is inhibited and magnetization is forced to change rotation.

Fig. 6(c) shows the variation of the resistive part of impedance (Z') with frequency. It has been clearly viewed from the pattern itself that Z' decreases with the increase in frequency for characterized sample. The decrement in the real part of impedance (Z') with the rise in frequency may be due to the increase in ac conductivity with rise in frequency. It is observed that Z' has higher values at lower frequencies and decreases monotonically with the rise in frequency, and attains a constant value at higher frequency part.

Fig. 6(d) shows the variation of reactive part of impedance (Z'') with frequency, which indicates the same behavior as that of Z'. It is seen that Z'' decreases with increasing frequency.

Fig. 6(e) shows the variation in ac conductivity with frequency for different compositions at room temperature. The ac conductivity gradually increases for all compositions with the increase in frequency. It has been reported that the ac conductivity gradually increases with the increase in frequency of the applied ac field because the increase in frequency enhances the migration of electron.

From Fig. 6(f) it is clear that dielectric dispersion as ε'' value of the sample shows a decrease with increase in frequency. The decrease in dielectric constant is rapid at low frequency, and becomes slow at higher frequencies, approaching to frequency independent behavior.

As a result of the electrochemical performance, it is clear that prepared membranes having definite ratio of binder containing less than 25% was mechanically unstable and if it is having more than the above percentage it also shows unstable binding [28,29]. It is due to the separation of exchanger particles by the binder through which the membrane carries some charges. However, electrolyte solutions separated by a membrane (which is fixed in the cell) having unequal concentration. It is driven by different chemical potential performing across the membrane by the concentration of the solution which indicated the nature of the fixed charge on the membranes [30].

Chemical stability of composite membrane was determined by incubating in acidic, alkaline, and strongly oxidant media such as 1 M HNO_3, 1 M NaCl,

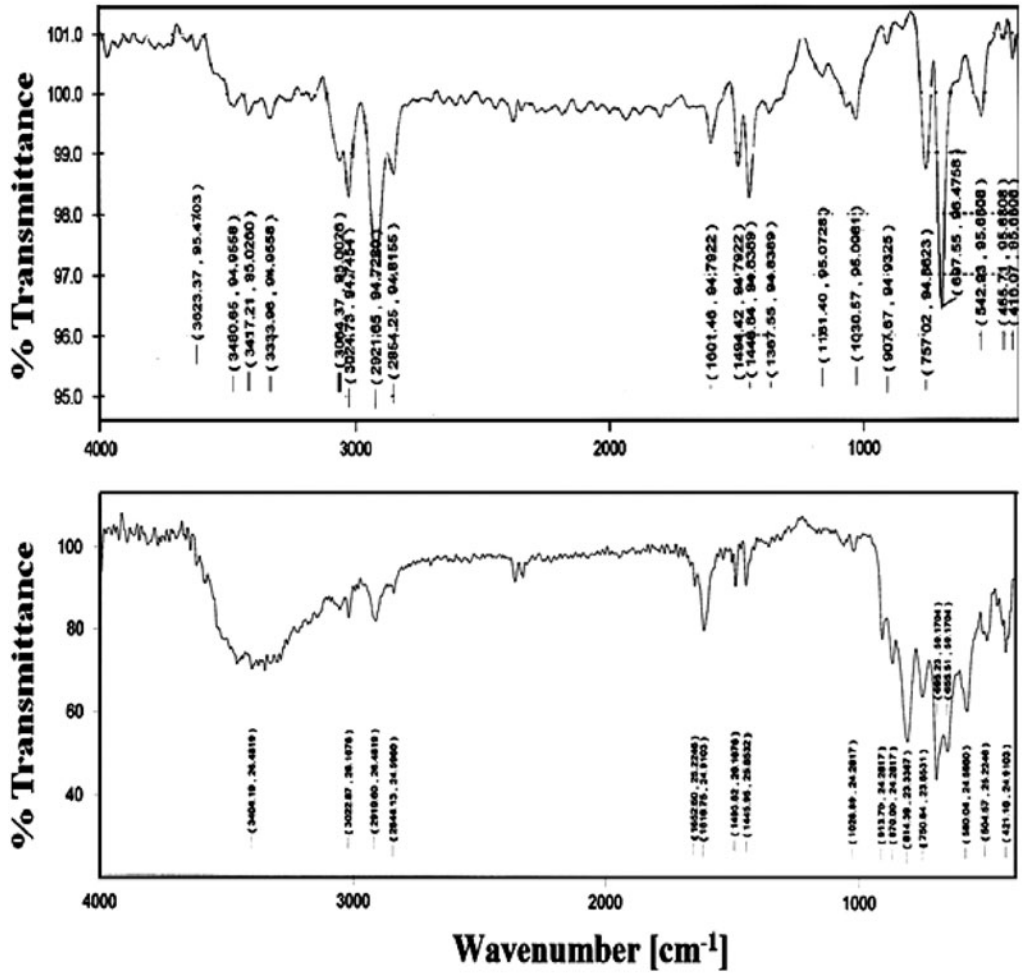

Fig. 4. FTIR spectra of pure polystyrene and polystyrene based MT composite membrane.

and 1 M NaOH solutions. By putting it into the above solutions for the 12, 24, 36, and 48 h the membrane lost their mechanical resistance which represent that the membrane is effective in such media. The high thermal stability, chemical stability, and the specificity of cations are the exclusive features of this composite membrane. The water content, thickness, porosity, and swelling are shown in Table 1.

Membrane potentials had been regarded for a long time as a measure of the membrane selectivity of different electrolyte solutions such as KCl, NaCl, and LiCl. The measurement of ion activity by means of membrane potential is more successful in the concentration range over which the membrane behaves as an ideally selective one, and hence, obeys the Nernst equation. From the observation, it is clear that the membrane potential decreases with an increase in external electrolyte's concentrations resulting membrane is ideally cation selective i.e. negatively charged which is depicted in Table 2.

The membrane under consideration seems to be truly selective and specific for K^+, Na^+, Li^+ and it was investigated by observing the membrane potentials in contact with KCl, NaCl, and LiCl solutions. The charge and nature of anion did not substantially influence the potentiometric response of the membrane. The potential data obtained for the composite membrane using various 1:1 electrolytes are plotted as a function of $-\log C_2$ in Fig. 7.

The activities electrolytic ions can be corrected by the Donnan potential through the integration of Planck or Henderson equation. According to TMS theory, the membrane potential is given by the equation at 25°C.

$$\Delta\overline{\Psi}_m = 59.2\left(\log\frac{C_2}{C_1}\frac{\sqrt{4C_1^2+\bar{D}^2}+\bar{D}}{\sqrt{4C_2^2+\bar{D}^2}+\bar{D}}+\bar{U}\log\frac{\sqrt{4C_2^2+\bar{D}^2}+\overline{DU}}{\sqrt{4C_1^2+\bar{D}^2}+\overline{DU}}\right) \quad (5)$$

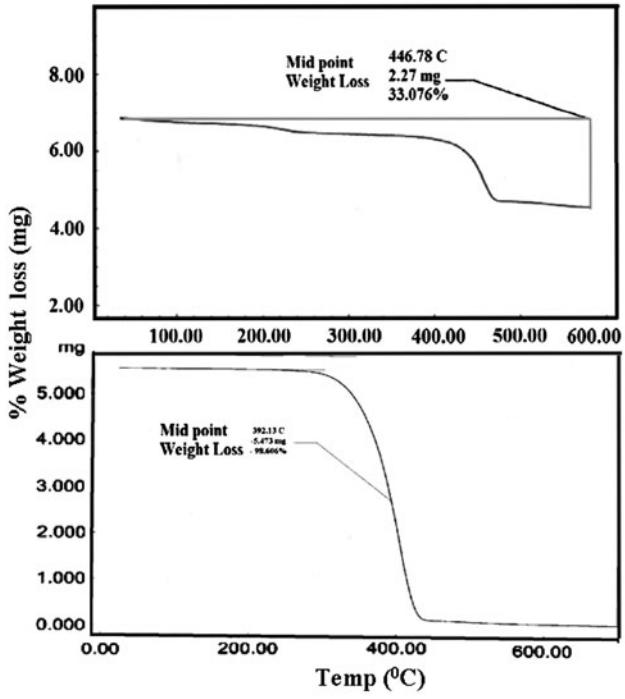

Fig. 5. TGA curve of polystyrene based MT composite membrane.

where

$$\bar{U} = (\bar{u} - \bar{v})/(\bar{u} - \bar{v})$$

where $\bar{u}$ and $\bar{v}$ are the ionic mobility of cations and anions ($m^2/v/s$), respectively, in the membrane phase, C_1 and C_2 are the concentrations of the membrane and $\bar{D}$ is the charge on the membrane expressed in equivalent per liter. The graphical method of TMS determines the fixed charge $\bar{D}$ in eq/L and the cation-to-anion mobility ratio in the membrane phase. Charged membrane was placed at the center of the potentials measuring cell, which has two glass chambers on either side of the membrane. The disparity in the selective nature of the membrane is due to the adsorption of particular ions which leads a condition in which the membrane surface making cation selective nature due to the presence of net negative charge on the membrane. The inorganic precipitate has the capacity to create potentials due to the interphase among electrolyte solutions of having different concentrations [31,32].

The charges of the membrane play a major role in the adsorption as well as transportation of electrolyte ions in synthetic as well as standard membranes. The most important electrochemical properties are permeability differences in the co ions, counter ions as well as neutral molecules. The potential of diluted electrolyte solution is dependent on the porosity of the membrane [33]. Therefore, without the evaluation of the thermodynamically-effective fixed-charge density the transport mechanism of electrolytes solution within the charged membrane appear to be incomplete.

If the membrane pores are broad it results that any sum of charge does to generate good potentials on the membrane. On the other hand, if the pores are narrow, a little quantity of charge can give rise to appropriate potential values. Therefore, it shows the transport mechanism of simple electrolytes within the charged membrane appear to be incomplete without the evaluation of the thermodynamically effective fixed charge density of the membrane [34,35]. The membranes carrying various charge densities which can be written as, $\bar{D} \leqslant 1$, the theoretical and observed potential showed by solid and broken line, respectively and were plotted as a function of $-\log C_2$ Fig. 8. Thus, the coinciding curves for various electrolytes system gave the value of the charge density $\bar{D}$ within the membrane phase (Table 3).

The surface charge density $\bar{D}$ of membrane is found to depend on the initial stage of preparation and the order of charge density was found to be KCl > NaCl > LiCl. The charge density is higher in the case of KCl than in the NaCl case due to the size factor of electrolyte. The TMS Eq. (5) can also be expressed by the sum of Donnan potential ($\Delta\Psi_{\text{Don}}$) among the membrane surfaces and the external solutions, and the diffusion potential ($\Delta\Psi_{\text{Diff}}$) within the membrane [36,37].

$$\Delta\bar{\Psi}_{m,e} = \Delta\bar{\Psi}_{\text{Don}} + \Delta\bar{\Psi}_{\text{diff}} \tag{6}$$

$$\Delta\bar{\Psi}_{\text{Don}} = -\frac{RT}{V_\kappa F}\ln\left(\frac{\gamma_{2\pm}C_2\bar{C}_{1+}}{\gamma_{1\pm}C_1\bar{C}_{2+}}\right) \tag{7}$$

where R, T, and F have their usual significance, $\gamma_{1\pm}$ and $\gamma_{2\pm}$ are the mean ionic activity coefficients, $\bar{C}_{1\pm}$ and $\bar{C}_{2\pm}$ are the cation concentration in the membrane phase first and second, respectively. The cation concentration is given by the equation:

$$\bar{C}_+ = \sqrt{\left(\frac{V_x\bar{D}}{2V_k}\right)^2\left(\frac{\gamma_\pm C}{q}\right)^2} - \frac{V_x\bar{D}}{2V_k} \tag{8}$$

where V_k and V_x denotes the valency of cation and fixed-charge group on the membrane matrix, where q is the charge effectiveness of the membrane and is defined by the following equation.

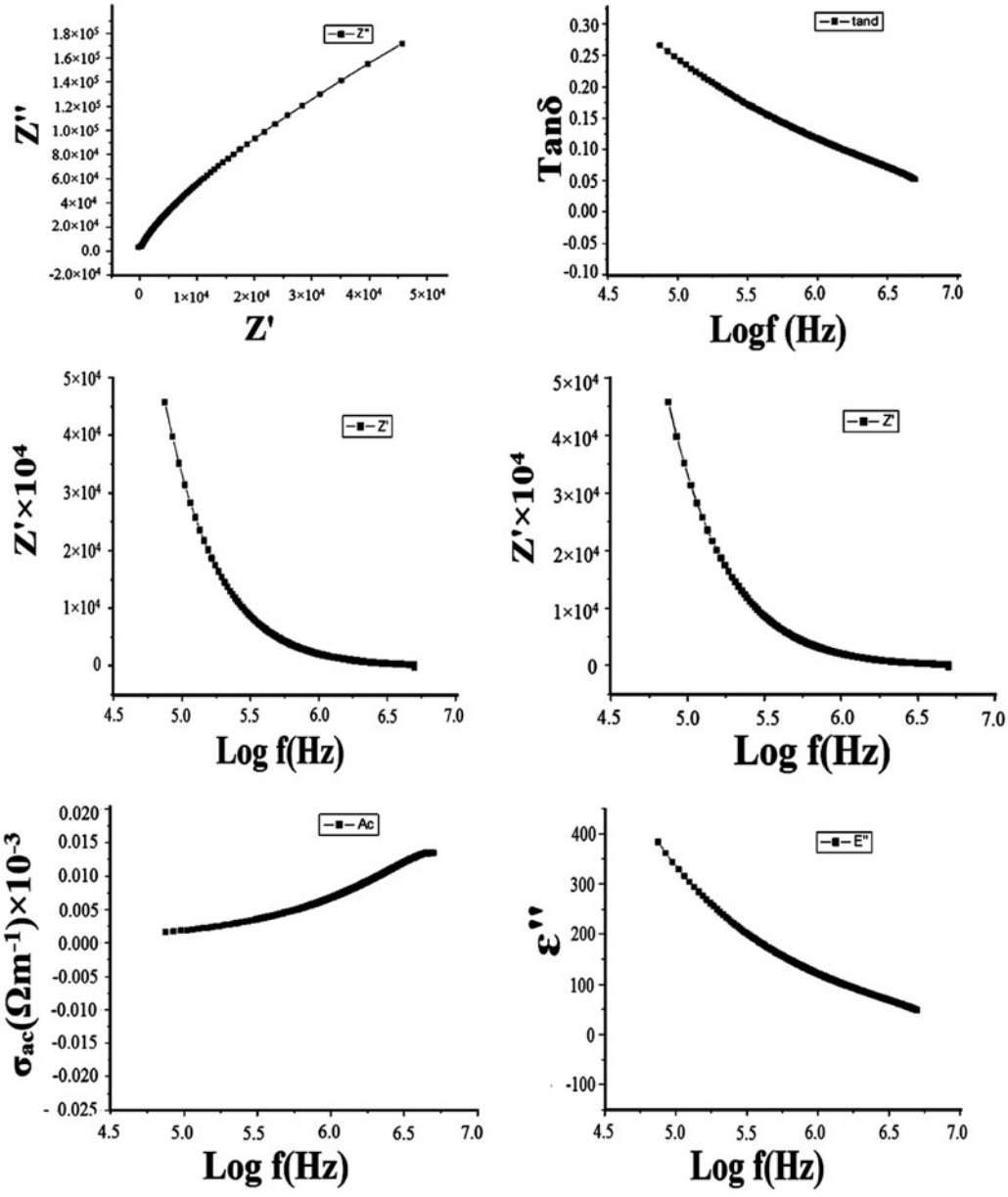

Fig. 6. (a)–(f) Dielectric properties of polystyrene based MT composite membrane.

Table 1
Thickness, water content, porosity and swelling properties of polystyrene based MT composite membnee

Applied pressure (MPa)	Thickness of membrane	Water content as % weight of wet membrane	Porosity	Swelling of % wet membrane
100	0.083	0.046	0.071	No swelling

$$q = \sqrt{\frac{\gamma_{\pm}}{K_{\pm}}} \tag{9}$$

where $K_{\pm}$ is the distribution coefficient expressed as:

$$K_{\pm} = \frac{\bar{C}_i}{C_i}, \quad \bar{C}_i = C_i - \bar{D} \tag{10}$$

where $\bar{C}_i$ is the ith ion concentration in the membrane phase and C_i is the ith ion concentration of the external solution. The diffusion potential, $\Delta\Psi_{\text{diff}}$ was expressed in the form

Table 2
Observed membrane potential in mV across the polystyrene based MT composite membrane in contact with various 1:1 electrolytes at different concentrations and pressures at 25 ± 1°C

Applied pressure 100 (MPa)			
Membrane potential (mV)			
Conc. (mol/L)	KCl	NaCl	LiCl
1	11.0	14.5	19.6
0.1	14.5	19.7	24.5
0.01	23.7	27.4	31.3
0.001	30.6	36.3	39.4
0.0001	39.5	44.6	50.9

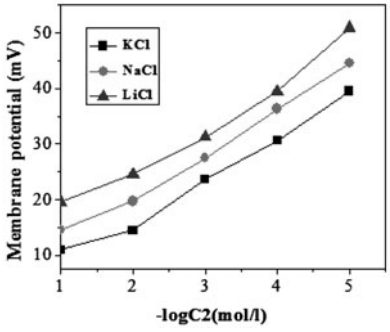

Fig. 7. Plots of observed membrane potentials against logarithm of concentration for polystyrene based MT composite membrane using various 1:1 electrolytes at 100 MPa.

$$\delta\bar{\Psi}_{diff} = -\frac{RT\bar{\omega}-1}{V_kF\bar{\omega}+1}\times\ln\left(\frac{(\bar{\omega}+1)\bar{C}_2+(V_X/V_k)D}{(\bar{\omega}+1)\bar{C}_1+(V_X/V_k)D}\right) \quad (11)$$

where $\bar{\omega}=\bar{u}/\bar{v}$ is the mobility ratio of the cation toward the anion in membrane phase. Therefore, total membrane potential $\Delta\bar{\Psi}_{m,e}$ was obtained by the following:

$$\Delta\bar{\Psi}_{m.e} = -\frac{RT}{V_kF}\ln\left(\frac{\gamma_{2\pm}C_2\bar{C}_{1\pm}}{\gamma_{1\pm}C_1\bar{C}_{2\pm}}\right)-\frac{RT\bar{\omega}-1}{V_kF\bar{\omega}+1}\times\ln\left(\frac{(\bar{\omega}+1)\bar{C}_2+(V_X/V_k)\bar{D}}{(\bar{\omega}+1)\bar{C}_1+(V_X/V_k)\bar{D}}\right) \quad (12)$$

$$\Delta\bar{\Psi}_m = -\frac{RT}{F}(t_+-t_-)\ln\frac{C_2}{C_1} \quad (13)$$

where

$$\frac{t_+}{t_-}=\frac{\bar{u}}{\bar{v}} \quad (14)$$

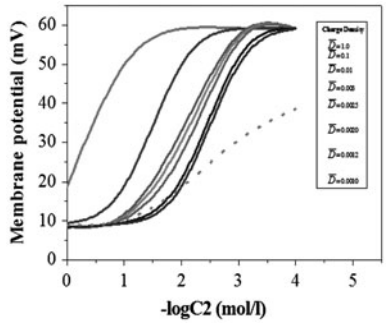

Fig. 8. Plots of membrane potential (theoretical and observed) (mV) vs. $-\log C_2$ (mol/L) at different concentrations of KCl electrolyte solution for polystyrene based MT composite membrane prepared at pressure of 100 MPa.

Table 3
Derived values of membrane charge density ($\bar{D}$, eq/l) for various polystyrene based MT composite membrane electrolyte system using TMS equation

Applied pressure (MPa)	KCl	NaCl	LiCl
100	0.0612	0.0403	0.0301

For the applicability of these theoretical equations for the system the Diffusion potential and Donnan potential were separately calculated from the membrane potential data by using a distinctive membrane at a pressure of 100 MPa [38].

To get the value of transport number, t_+ Eq. (13) will be used and t_- from experimental membrane potential data and consequently the mobility ratio $\bar{\omega}=\bar{u}/\bar{v}$ can also be calculated. The mobility of the electrolyte in the membrane phase were found to be high and follow the order of LiCl > NaCl > KCl as shown in Fig. 9. The high mobility is due to the higher transport number of comparatively free cations of electrolytes, whereas similar trend of mobility is also seen in the least-concentrated solution. The transport number of cation of the various electrolytes such as KCl, NaCl, and LiCl increases with decreasing the concentration of electrolytes and follows the increasing order KCl < NaCl < LiCl shown in Fig. 10.

Donnan and diffusion potential at various electrolyte concentrations can be calculated from the parameters $\gamma_{1\pm},\gamma_{2\pm},\bar{C}_{1+},\bar{C}_{2+},\bar{\omega},V_x,V_k$ and the experimentally derived values of charge density by using Eqs. (7) and (11). The values of the parameters, $K_{\pm q}$ and $\bar{C}_+$ are derived for the system and shown in Table 4. The values of $\gamma_\pm$ were the usual charted values for electrolyte KCl, NaCl, and LiCl.

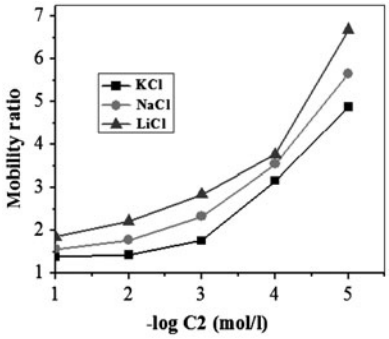

Fig. 9. The plot for mobility ratio of polystyrene based MT composite membrane for 1:1 electrolyte against concentration.

Table 4
The values of $t_+, \bar{U}, \bar{\omega}$ and $K_\pm, q, \bar{C}_+$ evaluated using Eqs. (9), (6), (5) and (4), respectively, from observed membrane potentials across various electrolytes at different concentrations for polystyrene based MT composite membrane

C_2 (mol/L)	t_+	$\bar{U}$	$\bar{\omega}$	$K_\pm$	q	$\bar{C}_+$
KCl (electrolyte)						
1.000	0.58	0.16	1.38	0.9388	1.065	0.9332
0.1000	0.59	0.18	1.43	0.388	2.577	0.0335
0.0100	0.66	0.32	1.76	−5.120	0.195	0.0458
0.0010	0.76	0.52	3.16	−60.20	0.0166	0.0548
0.0001	0.83	0.66	4.88	−611.00	0.0016	0.0570
NaCl						
1.000	0.61	0.22	1.56	0.9597	1.014	0.9805
0.1000	0.64	0.28	1.77	0.5970	1.675	0.0542
0.0100	0.70	0.40	2.33	−3.03	0.330	0.0251
0.0010	0.78	0.56	3.54	−39.30	0.025	0.0347
0.0001	0.85	0.70	5.66	−402.00	0.002	0.0446
LiCl						
1.000	0.65	0.30	1.85	0.9699	1.013	0.9814
0.1000	0.69	0.38	2.22	0.699	1.430	0.0644
0.0100	0.74	0.48	2.84	−2.01	0.497	0.0152
0.0010	0.79	0.58	3.76	−29.10	0.034	0.0242
0.0001	0.87	0.74	6.69	−300.0	0.0003	0.3276

5. Conclusion

The polystyrene-based MT composite membrane which was prepared by applying the theoretical approach mentioned above was found quite stable. Several conclusions are drawn as: The characterization structural details of the membrane showed great properties in terms of effective charge density, mobility ratio, membrane thickness, and membrane porosity.

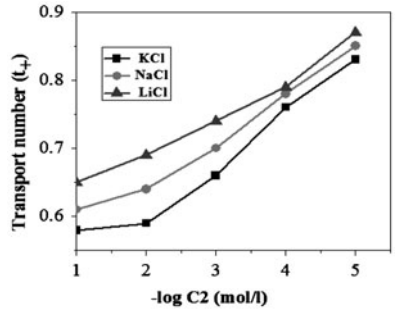

Fig. 10. plots showing the transport number of cation for the polystyrene based MT composite membrane for 1:1 electrolytes (KCl, NaCl, LiCl) vs. concentration.

The fixed-charge density is the central parameter for governing transport phenomena in membranes and depends upon the feed composition and applied pressure. The increase of electrolytes concentration tends to exhibit smaller membrane potential. The membrane potential for different 1:1 electrolytes was found to follow an increasing order KCl < NaCl < LiCl and surface charge density follows a reverse order. For upcoming works, this membrane model can be enhanced further to be acceptable and withstand in the range of the commercial membranes available in the markets.

Nomenclature

AR	analytical reagent
C_1, C_2	concentrations of electrolyte solution on either side of the membrane (mol/L)
$\bar{C}_{1+}$	cation concentration in membrane phase 1 (mol/L)
$\bar{C}_{2+}$	cation concentration in membrane phase 2 (mol/L)
C_i	*i*th ion concentration of external solution (mol/L)
$\bar{C}_i$	*i*th ion concentration in membrane phase (mol/L)
$\bar{D}$	charge density in membrane (eq/L)
F	Faraday constant (C/mol)
100 MPa	pressure (MPa)
q	charge effectiveness of the membrane
R	gas constant (J/K/mol)
SCE	saturated calomel electrode
TMS	Teorell, Meyer and Sievers
t_+	transport number of cation
t_-	transport number of anion
$\bar{u}$	mobility of cations in the membrane phase ($m^2/v/s$)
$\bar{v}$	mobility of anions in the membrane phase ($m^2/v/s$)
V_k	valency of cation

V_x	valency of fixed-charge group
$\bar{U}$	$\bar{U} = (\bar{u} - \bar{v})/(\bar{u} + \bar{v})$
MT	manganous tungstate
SEM	scanning electron microscopy
FTIR	Fourier transform infrared spectroscopy
XRD	X-ray diffraction
TGA	thermogravimetric analysis
DTA	differential thermal analysis
LCR	inductance, capacitance, and resistance

Greek symbols

$\gamma_{\pm}$	mean ionic activity coefficients
$\bar{\omega}$	mobility ratio
$\Delta\psi_m$	observed membrane potential (mV)
$\Delta\bar{\Psi}_m$	theoretical membrane potential (mV)
$\Delta\Psi_{\text{Don}}$	Donnan potential (mV)
$\Delta\bar{\Psi}_{\text{diff}}$	Diffusion potential (mV)

Acknowledgment

The authors gratefully acknowledge the Chairman, Department of Chemistry, and Aligarh Muslim University, Aligarh (India) for providing necessary research facilities for FTIR, LCR, and TGA/DTA analysis. We are also thankful to the UGC for providing financial assistance, Center of Excellence in Materials Science-Department of Applied Physics AMU Aligarh to provide XRD facility and USIF-AMU Aligarh for Scanning electron microscope facility.

References

[1] R.K. Nagarale, V.K. Shahi, S.K. Thampy, R. Rangarajan, Studies on electrochemical characterization of polycarbonate and polysulfone based heterogeneous cation-exchange membranes, React. Funct. Polym. 61 (2004) 131–138.
[2] G.S. Gohil, R.K. Nagarale, V.V. Binsu, V.K. Shahi, Preparation and characterization of monovalent cation selective sulfonated poly (ether ether ketone) and poly (ether sulfone) composite membranes, J. Colloid Interface Sci. 298 (2006) 845–853.
[3] T.J. Chou, A. Tanioka, Ionic behavior across charged membranes in methanol water solutions. I: Membrane potential, J. Membr. Sci. 144 (1998) 275–284.
[4] W. Cuiming, X. Xinle, C. Peng, X. Tongwen, Preparation and applications of hybrid ion exchange membranes, Prog. Chem. 22 (2010) 2003–2013.
[5] M.R. Ladisch, K.L. Kohlmann, Recombination of human insulin, Biotechnol. Prog. 8 (1992) 469–478.
[6] S. Khemakhem, R.B. Amara, Purification of industrial effluent by microfiltration and ultra filtration ceramic membranes: Comparative study between commercial and elaborated Tunisian clay membranes, Desalin. Water Treat. 39 (2012) 182–189.
[7] X. Zhu, W. Yang, Composite membrane based on ionic conductor and mixed conductor for oxygen permeation, AIChE J. 54 (2008) 665–672.
[8] T. Arfin, Rafiuddin, An electrochemical and theoretical comparison of ionic transport through a polystyrene-based cobalt arsenate membrane, J. Electrochim. Acta 56 (2011) 7476–7483.
[9] A.A. Khan, U. Habiba, A. Khan, Synthesis and characterization of organic-inorganic nanocomposite poly-o-anisidine Sn (IV) arsenophosphate: Its analytical applications as Pb(II) ion-selective membrane electrode, Int. J. Anal. Chem. 10 (2009), doi: 10.1155/2009/659215.
[10] K.G. Varshney, A. Agrawal, S.C. Mojumdar, Pyridine based thorium(IV)phosphate hybride fibous ion exchanger, synthesis, characterization and thermal behavior, J. Therm. Anal. Calorim. 90 (2007) 721–724.
[11] A.P. Gupta, G.L. Verma, H. Aggarwal, Polyvinylchloride membrane containing zirconium(IV) selenomolybdate inorganic ion exchanger as ion selective electrolyde, Indian J. Chem. 42 (2003) 1910–1913.
[12] A.A. Khan Inamuddin, M.M. Alam, Determination and separation of Pb^{2+} from aqueous solutions using a fibrous type organic-inorganic hybrid cation-exchange material: Polypyrrole thorium(IV) phosphate, React. Funct. Polym. 63 (2005) 119–133.
[13] R. Niwas, A.A. Khan, K.G. Varshney, Synthesis and ion exchange behaviour of polyaniline Sn(IV) arsenophosphate: A polymeric inorganic ion exchanger, Colloids Surf. A 150 (1999) 7–14.
[14] M. Arsalan, M.M.A. Khan, Rafiuddin, A comparative study of theoretical, electrochemical and ionic transport through PVC based $Cu_3(PO_4)_2$ and polystyrene supported $Ni_3(PO_4)_2$ composite ion exchange porous membranes, Desalination 318 (2013) 97–106.
[15] F.J. Helfferich, Ion Exchange, 9th ed., McGraw-Hill, New York, NY, 425 1962.
[16] N. Lakshminarayanaiah, Transport Phenomena in Membranes, Academic Press, New York, NY, 1969.
[17] T.J. Chou, A. Tanioka, Membrane potential of composite bipolar membrane in ethanol–water solutions-the role of the membrane interface, J. Colloid Interface Sci. 212 (1999) 293–300.
[18] Y. Tomoko, I. Shinya, H. Mitsuru, Transport properties of ions through temperature-responsive charged membranes prepared using poly(vinyl alcohol)/poly(N-isopropylacrylamide)/poly(vinylalcohol-co-2-acrylamido-2 methyl propane sulfonic acid), J. Membr. Sci. 250 (2005) 61–68.
[19] M. Higa, A. Taniokaa, A. Kira, A novel measurement method of Donnan potential at an interface between a charged membrane and mixed salt solution, J. Membr. Sci. 140 (1998) 213–220.
[20] M.A. Ansari, M. Kumar, N. Singh, K.S. Dadoriya, R.S. Kushwaha, S. Ayub, Ion transport studies through polystyrene based model membrane: Conductance data and absolute reaction rate theory, Adv. Appl. Sci. Res. 3 (2012) 251–260.
[21] F. Jabeen Rafiuddin, Rafiuddin Preparation and development of the surface charge density of vanadium phosphate membranes in electrolyte solutions, J. Appl. Polym. Sci. 110 (2008) 3023–3030.
[22] F. Jabeen, Rafiuddin Membrane potential and fixed charge density across TiPO4–VPO4 composite membranes for uni-univalent electrolyte solution, J. Porous Mater. 16 (2009) 257–265.
[23] J. Zhao, D. Wu, Y. Sun, Z. Zhang, H. Zhang, D. Zhao, Synthesis and characterizations of mesoporous zirconia-based oxide composites, Stud. Surf. Sci. Catal. 135 (2001) 250.
[24] M.M.A. Khan, Rafiuddin, Preparation, characterization, biological activity, and transport study of polystyrene based calcium–barium phosphate composite membrane, Mat. Sci. Eng. C 33 (2013) 4228–4235.
[25] W. Liang, W.C. Tongwen, C.W. Dan, X. Zheng, Preparation and characterization of CPPO/BPPO blend membranes for potential application in alkaline direct methanol fuel cell, J. Membr. Sci. 310 (2008) 577–585.
[26] H. Haibo, G. Bin, C. Feng, Effect of membrane surface characterization on salt and water transport through aromatic polyamide membranes, Adv. Sci. Lett. 12 (2012) 218–222.

[27] ASTM D543–95, Standard Particles for Evaluating the Resistance of Plastics to Chemical Reagents, Standard, 27 (1998).
[28] T. Arfin, Rafiuddin Transport studies of nickel arsenate membrane, J. Electroanal. Chem. 636 (2009) 113–122.
[29] M.M.A. Khan, Rafiuddin Metal ion transport through a polystyrene-based cobalt arsenate membrane: Application of irreversible thermodynamics and theory of absolute reaction rates, Desalination 284 (2012) 100–105.
[30] A. Kruissink, Bergsma, ion-exchange membranes, Adv. Polym. Sci. 2(1) (1960) 307–362.
[31] V.K. Shahi, G.S. Trivedi, S.K. Thampy, R. Ranrarajan, Studies on the electrochemical and permeation characteristics of asymmetric charged porous membranes, J. Colloid Interface Sci. 262 (2003) 566–573.
[32] M.M.A. Khan, Rafiuddin Synthesis, characterization and electrochemical study of calcium phosphate ion-exchange membrane, Desalination 272 (2011) 306–312.
[33] M.M. Nasef, H. Saidi, Structure of polyethylene-graft-polystyrene sulfonic acid membranes prepared by radiation-induced grafting, Int. J. Polym. Mater. 53 (2004) 1–17.
[34] A.M. Hollman, N.T. Scherrer, A.C. Goodwin, D. Bhattacharyya, Separation of dilute electrolytes in poly(amino acid) functionalized microporous membranes: Model evaluation and experimental results, J. Membr. Sci. 239 (2004) 65–79.
[35] T. Arfin, Rafiuddin Electrochemical properties of titanium arsenate membrane, J. Electrochim. Acta 54 (2009) 6928–6934.
[36] H. Matsumoto, A. Tanioka, T. Murata, M. Higa, K. Horiuchi, Effect of proton on potassium ion in counter transport across fine porous charged membranes, J. Phys. Chem. B 102 (1998) 5011–5016.
[37] T.J. Chou, A. Tanioka, Membrane potential of composite bipolar membrane in ethanol–water solutions, the role of the membrane interface, J. Colloid Interface Sci. 212 (1999) 293–300.
[38] R. Wycisk, P.N. Pintauro, Sulfonated polyphosphazene ion-exchange membranes, J. Membr. Sci. 119 (1996) 155–160.